Disease Models & Mechanisms 2, 283-294 (2009) doi:10.1242/dmm.002287

Multiple congenital malformations of Wolf-Hirschhorn syndrome are recapitulated in *Fgfrl1* null mice

Catarina Catela[1], Daniel Bilbao-Cortes[1], Esfir Slonimsky[1], Paschalis Kratsios[1], Nadia Rosenthal[1] and Pascal te Welscher[1,*]

SUMMARY

Wolf-Hirschhorn syndrome (WHS) is caused by deletions in the short arm of chromosome 4 (4p) and occurs in about one per 20,000 births. Patients with WHS display a set of highly variable characteristics including craniofacial dysgenesis, mental retardation, speech problems, congenital heart defects, short stature and a variety of skeletal anomalies. Analysis of patients with 4p deletions has identified two WHS critical regions (WHSCRs); however, deletions targeting mouse WHSCRs do not recapitulate the classical WHS defects, and the genes contributing to WHS have not been conclusively established. Recently, the human *FGFRL1* gene, encoding a putative fibroblast growth factor (FGF) decoy receptor, has been implicated in the craniofacial phenotype of a WHS patient. Here, we report that targeted deletion of the mouse *Fgfrl1* gene recapitulates a broad array of WHS phenotypes, including abnormal craniofacial development, axial and appendicular skeletal anomalies, and congenital heart defects. *Fgfrl1* null mutants also display a transient foetal anaemia and a fully penetrant diaphragm defect, causing prenatal and perinatal lethality. Together, these data support a wider role for *Fgfrl1* in development, implicate *FGFRL1* insufficiency in WHS, and provide a novel animal model to dissect the complex aetiology of this human disease.

INTRODUCTION

Wolf-Hirschhorn Syndrome (WHS) is a contiguous gene disorder that results in craniofacial defects, microcephaly, mental retardation, congenital heart defects, problems in the development of speech, respiratory diseases, intra-uterine and postnatal growth retardation, and short stature, in combination with multiple skeletal anomalies (Battaglia et al., 2001). WHS is estimated to occur in about one in every 20,000 births (Maas et al., 2008). Correlations between the highly variable phenotypes of patients with WHS and their genotypes show that the disease is generally caused by deletions of the short arm of chromosome 4 (4p) (Bergemann et al., 2005). Approximately 20% of cases carry chromosomal deletions that are restricted to 4p16.3, but larger deletions are more common and can extend as far as 4p14.

The comparison between interstitial and 4p terminal deletions resulted in the identification of two WHS critical regions (WHSCR-1 and -2) that are approximately 2 Mb from the telomeric end of the chromosome, and two genes located at this site have since been referred to as the Wolf-Hirschhorn syndrome candidate 1 (*WHSC1*) and 2 (*WHSC2*) genes. Haploinsufficiency of *WHSC1* is considered to be responsible for the typical craniofacial phenotype ('Greek helmet face') that is present in almost all WHS patients, but mouse models for WHS show that deletions targeting the WHSCRs on the mouse chromosome do not recapitulate the classical WHS defects (Näf et al., 2001). Instead, the fibroblast growth factor receptor-like 1 (*FGFRL1*) gene, located at 4p16.3, has been implicated recently as an important candidate gene contributing to the craniofacial phenotype of a WHS patient carrying a small telomeric deletion in chromosome 4 that included the *FGFRL1* locus but left the WHSCRs unaffected (Engbers et al., 2009). A role for *FGFRL1* in human craniofacial development is supported further by the characterisation of a FGFRL1 mutation in a patient with craniosynostosis (Rieckmann et al., 2009). Small telomeric deletions of chromosome 4 that exclude the WHSCRs but include *FGFRL1* have also been associated with intra-uterine growth retardation and short stature in WHS patients (Maas et al., 2008). As *Fgfrl1* is preferentially expressed in skeletal tissues and is prominent in the primordia of the maxillae, the mandibles and the permanent cartilage of the trachea and nose during late stages of mouse development (Trueb and Taeschler, 2006; Trueb et al., 2003), these data collectively point towards a potential role for *FGFRL1* in craniofacial development and suggest that haploinsufficiency of *FGFRL1* in humans with 4p16.3 deletions may contribute to the WHS craniofacial phenotype.

The fibroblast growth factor (FGF) family comprises a complex signalling system involving 22 different ligands in humans and mice that interact with tissue-specific splice variants of four different FGF receptors (FGFRs) to coordinate a wide range of cellular and developmental processes (Bottcher and Niehrs, 2005; Thisse and Thisse, 2005). The independent identification of the FGFRL1 protein by several research groups added a potential component to the FGF signalling system (Kim et al., 2001; Sleeman et al., 2001; Wiedemann and Trueb, 2000; Wiedemann and Trueb, 2001). The predicted extracellular domain of FGFRL1 is highly related to the FGFRs, which are cell surface receptor tyrosine kinases with three extracellular immunoglobulin-like domains and a heparin-binding sequence, but FGFRL1 lacks the intracellular protein tyrosine kinase domain that is essential for FGF signal transduction. Although FGFRL1 might not directly activate an intracellular signalling cascade, in vitro assays show that FGFRL1 interacts with FGF ligands and heparin, and thus may function as a decoy receptor in the FGF signalling pathway (Sleeman et al., 2001; Trueb et al., 2003). A single *Fgfrl1* gene was found in mammalian (Sleeman et al., 2001), bird (Trueb et al., 2003) and amphibian (Hayashi et al., 2004) species, as well as in the cephalochordate *Brachiostoma floridae* (Beyeler and Trueb,

[1]European Molecular Biology Laboratory, Mouse Biology Unit, 00015 Monterotondo, Italy
*Author for correspondence (e-mail: welscher@embl.it)

2006), suggesting that the *Fgfrl1* gene predates the two genome duplications that occurred early in vertebrate evolution. In fish species such as zebrafish and *Fugu rubripes*, two copies of the *Fgfrl1* gene can be found (Trueb et al., 2005), which is in line with the additional genome duplication during the evolution of ray-finned fish. Functional studies in zebrafish provided in vivo evidence for an essential role of *Fgfrl1* in vertebrate craniofacial skeletal development (Hall et al., 2006). Depletion of zebrafish *fgfrl1a* and *fgfrl1b* results in a craniofacial phenotype, including malformations of the lower jaw and developmental inhibition of the cartilage formed by the branchial arches, and the authors propose that *fgfrl1a* is required for FGF signal transduction to promote gill cartilage formation. *Fgfrl1*-deficient mice, generated by Baertschi et al. (Baertschi et al., 2007), unexpectedly did not reveal any defects in skeletal development. Instead, these *Fgfrl1*-deficient mice display a prominent diaphragm defect and fail to inflate their lungs after birth, causing perinatal lethality.

To facilitate the analysis of *Fgfrl1* function in more detail, we generated an *Fgfrl1* mutant allele, targeting different exons from those described by Baertschi et al. (Baertschi et al., 2007). The *Fgfrl1* null mice display a broad array of phenotypes, including cardiac abnormalities and skeletal malformations. Defects in cardiac development and foetal anaemia probably caused the prenatal lethality that was observed in a subpopulation of $Fgfrl1^{-/-}$ mutants. The diaphragm phenotype described by Baertschi et al. (Baertschi et al., 2007) was fully penetrant in the $Fgfrl1^{-/-}$ mice that develop until term and, together with the defects in cardiac and skeletal development, caused perinatal lethality. These congenital malformations underscore the crucial function of *Fgfrl1* in embryonic development. The significant overlap of the phenotype of *Fgfrl1* null mice with clinical WHS presentations confirms a central role for *FGFRL1* in the human syndrome and implicates a gene outside of the WHSCRs in the WHS phenotype. *Fgfrl1* null mice thus provide a model to study FGFRL1 activity in FGF signalling and to dissect the complex aetiology of WHS.

RESULTS

Developmental expression of *Fgfrl1*

Expression of *Fgfrl1* has been well described by Trueb et al. (Trueb et al., 2006) for 15- to 17-day-old mouse embryos, but to evaluate an earlier role for this receptor we studied *Fgfrl1* expression by whole-mount in situ hybridisation during early developmental stages. At embryonic day (E)10.5, a wide range of tissues expressed *Fgfrl1* including brain, cranial placodes, pharyngeal arches and somites (Fig. 1A). A cross section through the otic vesicle, the first two pharyngeal arches and the nasal pit showed *Fgfrl1* expression in the cranial placodes and in a subepithelial compartment of the pharyngeal arches (Fig. 1B). *Fgfrl1* was also expressed at a medial site of the hindbrain and expression in the central nervous system extended from the brain to the neural tube (Fig. 1C). The heart was another prominent site of *Fgfrl1* expression at E10.5 (Fig. 1D). Transverse sections confirmed a very specific expression pattern of *Fgfrl1* in the endocardial cushions of the atrioventricular canal (Fig. 1E) and the cardiac outflow tract (Fig. 1F).

Fgfrl1 null mice display both prenatal and perinatal lethality

To delineate the function of *Fgfrl1* in embryonic development and its potential role in WHS, we generated mice carrying $Fgfrl1^{flox}$, in which the DNA segment that includes exons 3 to 7 was flanked by *loxP* sites (Fig. 2A-C). $Fgfrl1^{flox/+}$ mice, as well as recombined $Fgfrl1^{+/-}$ heterozygotes, were viable and fertile with no discernible phenotype. Quantification of *Fgfrl1* mRNA levels in E12.5 $Fgfrl1^{-/-}$ embryos confirmed the absence of *Fgfrl1* expression, indicating that the recombined allele is a true null allele (Fig. 2D). *Fgfr3*, *Whsc1* and *Whsc2* are located within the WHSCRs and have been linked to WHS characteristics (Bergemann et al., 2005), but mRNA levels of these genes showed no significant differences between wild-type and $Fgfrl1^{-/-}$ embryos. This excludes the possibility that changes in the expression levels of these WHSCR genes contribute to the mutant phenotype. $Fgfrl1^{-/-}$ embryos were still present at the expected Mendelian ratio at age E18.5 (Table 1). At E14.5 no gross

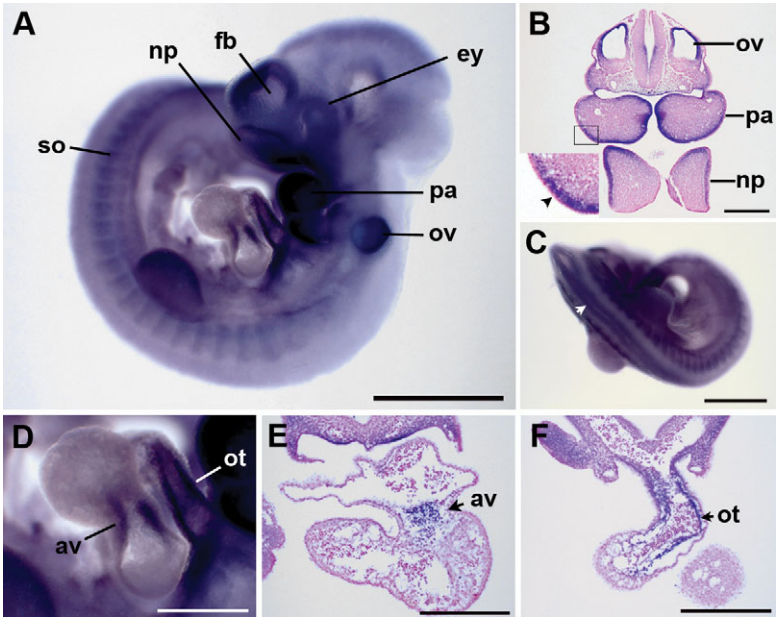

Fig. 1. Expression of *Fgfrl1* at age E10.5. (A) *Fgfrl1* expression is prominent in the brain, cranial placodes, pharyngeal arches and somites. (B) Cross section through the otic vesicle, first and second pharyngeal arches and nasal pit confirms *Fgfrl1* expression in the cranial placodes, as well as in a subepithelial compartment of the pharyngeal arch (inset; arrowhead indicates the pharyngeal ectoderm without *Fgfrl1* expression). (C) *Fgfrl1* expression in the neural tube (arrowhead). (D-F) *Fgfrl1* expression in the heart (D) and in the endocardial cushions (arrows) of the atrioventricular canal (E) and cardiac outflow tract (F). Abbreviations: av, atrioventricular canal; ey, eye; fb, forebrain; np, nasal pit; ot, outflow tract; ov, otic vesicle; pa, pharyngeal arch; so, somite. Bars, 1 mm (A,C); 0.5 mm (B,D-F).

morphological distinction was detected between *Fgfrl1*$^{-/-}$ foetuses and their wild-type littermates (Fig. 3A,B), but at E16.5 a subpopulation of the *Fgfrl1*$^{-/-}$ embryos suffered prenatal death, displaying developmental retardation and defective formation of the vascular system (Fig. 3C-E). The vascular defect was also evident in the yolk sac (Fig. 3F,G). Mildly affected *Fgfrl1*$^{-/-}$ embryos could be distinguished from wild-type littermates because of their dome-shaped cranium and short stature (Fig. 3C,D). By E18.5, the subpopulation (approximately 40%) of severely affected homozygotes had completely deteriorated, whereas the *Fgfrl1*$^{-/-}$ embryos that remained at age E18.5 developed until term (Fig. 3H). Surviving *Fgfrl1*$^{-/-}$ neonates were smaller than their wild-type littermates and showed signs of severe respiratory distress, dying immediately after birth or surviving for only several hours. Histological analysis of the lungs of *Fgfrl1*$^{-/-}$ embryos at E18.5 did not reveal any morphological defects compared with wild-type littermates (data not shown) but, similar to previous findings by Baertschi et al. (Baertschi et al., 2007), *Fgfrl1*$^{-/-}$ embryos displayed a severe diaphragm phenotype (Fig. 3I,J) that caused perinatal lethality.

To determine whether the variable expressivity of the *Fgfrl1*$^{-/-}$ phenotype was affected by gender, we examined the sex distribution among the severely affected *Fgfrl1*$^{-/-}$ mutant embryos and those *Fgfrl1*$^{-/-}$ embryos that developed until term (Table 2). Near-equal distributions of males and females in both mutant subpopulations indicated that the variable expressivity of the *Fgfrl1*$^{-/-}$ phenotype is not related to gender.

Skeletal malformations in *Fgfrl1* null mice

Previous studies reported that *Fgfrl1* is primarily expressed in cartilaginous tissues and bone primordia (Trueb and Taeschler, 2006; Trueb et al., 2003). Since craniofacial features are a common

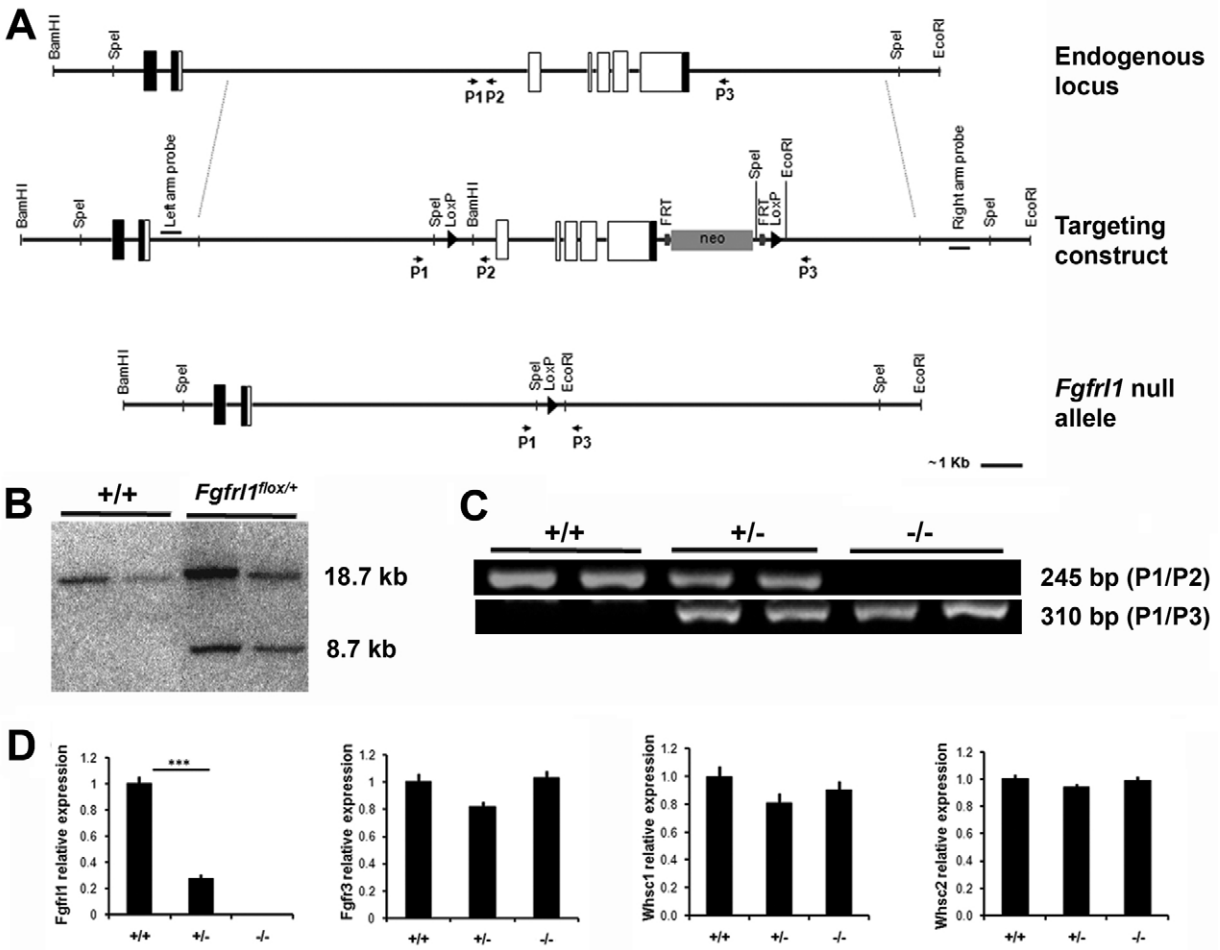

Fig. 2. Targeting of *Fgfrl1* by homologous recombination to produce the *Fgfrl1* null allele. (A) Schematic representation of the *Fgfrl1* locus, targeting construct and *Fgfrl1* null allele after Cre-mediated recombination of the targeted locus. Coding exons are depicted as open boxes and the 3′ and 5′ UTRs (untranscribed regions) are shown as black boxes. The *FRT*-flanked PGK *neo*^{r} cassette is depicted as a grey box. *LoxP* sites in the targeting construct flank exons 3-7 and the PGK *neo*^{r} cassette, which are removed after Cre-mediated deletion. Left arm and right arm external probes were used for screening embryonic stem (ES) cells to distinguish the endogenous allele from the targeted allele. Arrows indicate the position of the PCR primers (P1, P2, P3) used for genotyping. (B) Southern blot analysis using the left arm probe on ES cell genomic DNA after *Spe*I digest, indicating the wild-type (18.7 kb) and the *Fgfrl1*^{flox} allele (8.7 kb) in successfully targeted clones. (C) PCR analysis of embryos derived from matings between mice that are heterozygous for the *Fgfrl1* null allele, showing the 245 bp wild-type band and the 310 bp band of the *Fgfrl1* null allele. (D) Relative quantification of mRNA levels by RT-PCR for *Fgfrl1*, and the WHSCR genes *Fgfr3*, *Whsc1* and *Whsc2* in E12.5 embryos. Values are shown as fold induction in *Fgfrl1* mutants relative to wild-type littermates following normalisation to *Gapdh* expression (mean±s.e.m.). ***P<0.01.

Table 1. Genotype distribution in *Fgfrl1* mutant mice during development

	E14.5 (15 litters)	E16.5 (17 litters)		E18.5 (19 litters)		NB (28 litters)
Wild type	32 (26%)	35 (24%)		35 (24%)		55 (30%)
Heterozygous	56 (46%)	74 (51%)		77 (53%)		117 (63%)
Homozygous	33 (27%)	37 (25%)		33 (23%)		14 (7%)
		Severe	Mild	Severe	Mild	
		16	21	13	20	

hallmark of all WHS patients and a large variety of skeletal anomalies are found in up to 70% of individuals with WHS (Battaglia et al., 2001), we investigated skeletal development in those *Fgfrl1* null mice that develop until term. Alcian Blue and Alizarin Red S staining of *Fgfrl1*$^{-/-}$ E18.5 mutants revealed hypoplasia of all skeletal elements, including shortened axial and appendicular skeletons, malformed vertebrae, a small pelvic girdle and a small rib cage, in line with typical WHS skeletal phenotypes (Fig. 4A). At E18.5, the distance between the growth plates of the long bones in *Fgfrl1*$^{-/-}$ mice was reduced by 19-26% compared with in wild-type littermates (Table 3). The skeleton of *Fgfrl1*$^{-/-}$ mice also displayed an unusual large gap between the atlas and the occipital bone, in some cases resulting in the bulging of the spinal cord that was evident upon dissection. Closer examination of the head revealed an anterior-displaced foramen magnum in combination with severe hypoplasia and delayed fusion of the sphenoid, basisphenoid, and basioccipital bones that make up the cranial base of the skull (Fig. 4B). A dorsal view of the head showed that the calvarial elements in *Fgfrl1*$^{-/-}$ mice appeared thin, with a defect in suture closure (Fig. 4C). Midfacial hypoplasia, together with the round-headed appearance and an anterior shift of the foramen magnum in *Fgfrl1*$^{-/-}$ mice, was reminiscent of the achondroplasia-like phenotype in transgenic mice that express a constitutively active mutant of the MAP kinase kinase MEK1 in chondrocytes (Murakami et al., 2004). Forebrain development was also severely affected in *Fgfrl1*$^{-/-}$ mice (Fig. 4D,E), consistent with the observation that forebrain defects, mental retardation and facial dysgenesis, which are common in WHS and other subtelomeric deletion syndromes, are often genetically linked (Bergemann et al., 2005). Other phenotypes that overlap with WHS skeletal anomalies (Magill et al., 1980) included a delay in the ossification of the cervical vertebrae (Fig. 4F,G) and abnormal sternal ossifications (Fig. 4H,I) in association with a reduced thoracic diameter (Fig. 4A).

Fgfrl1 is expressed in the pharyngeal arches of mice (this study), zebrafish (Hall et al., 2006) and Xenopus (Hayashi et al., 2004). In zebrafish, *fgfrl1a* and *fgfrl1b* are essential for craniofacial development and, in particular, for the formation of gill cartilage derived from the branchial arches (Hall et al., 2006). Laryngeal

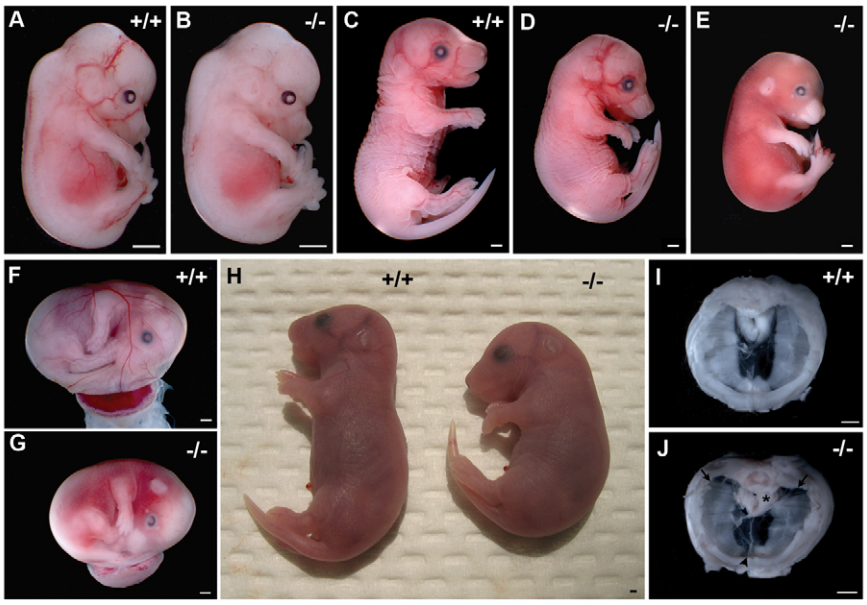

Fig. 3. Comparison between *Fgfrl1* wild-type (+/+) mice and homozygous mutant (–/–) mice. Wild-type (A) and *Fgfrl1*$^{-/-}$ (B) embryos at age E14.5 showed no gross morphological differences. Wild-type (C) and *Fgfrl1*$^{-/-}$ (D,E) embryos at age E16.5. At this stage, a subpopulation of *Fgfrl1*$^{-/-}$ embryos (E) was severely affected, suffering prenatal lethality and showing developmental retardation. Mildly affected *Fgfrl1*$^{-/-}$ embryos (D) display a short stature and a dome-shaped cranium. Wild-type (F) and severely affected *Fgfrl1*$^{-/-}$ (G) embryos at age E16.5 within their yolk sac. Whereas the yolk sac of the wild-type embryo (F) shows a prominent vasculature, the yolk sac of the *Fgfrl1*$^{-/-}$ embryo (G) lacks a clear vasculature and is devoid of blood. (H) Wild-type and mildly affected *Fgfrl1*$^{-/-}$ embryos at age E18.5. The *Fgfrl1*$^{-/-}$ embryos at this stage maintain the typical cranial and short stature phenotype. Comparison between the diaphragm from a wild-type (I) and *Fgfrl1*$^{-/-}$ (J) embryo at age E18.5 shows that the lumbar (arrows) and sternal (arrowhead) muscle portions of the diaphragm were not present in *Fgfrl1*$^{-/-}$ embryos and that the remaining costal portions of the diaphragm muscle were very thin in these embryos compared with in their wild-type littermates. The crural muscles (asterisk) in *Fgfrl1*$^{-/-}$ mice were also smaller compared with control animals and confirm the overall defect in diaphragm development. Bars, 1 mm.

Table 2. Sex distributions among *Fgfrl1*$^{-/-}$ mice

	Male	Female
Severely affected mutants	8 (53%)	7 (47%)
Mildly affected mutants	12 (44%)	15 (56%)
Total number of *Fgfrl1*$^{-/-}$ mice	**20 (48%)**	**22 (52%)**

cartilage elements that express *Fgfrl1* in mice (Trueb and Taeschler, 2006) also derive from the pharyngeal arches and were affected in the *Fgfrl1*$^{-/-}$ background. The hyoid bone was small and often incompletely ossified, and the thyroid and cricoid cartilages were significantly reduced in size (Fig. 4J,K). The affected laryngeal cartilage elements in *Fgfrl1*$^{-/-}$ mice also provide an explanation for the problems in swallowing and speech development in infants with WHS (Battaglia et al., 2001) and, in combination with the diaphragm phenotype, might contribute to respiratory distress (van Dooren et al., 2004).

Fgfrl1 is essential for the formation of cardiac valves and ventricular septation

The defective blood distribution in severely affected *Fgfrl1*$^{-/-}$ embryos and their yolk sac led us to focus on the development of the cardiovascular system. At E12.5, cardiac development in *Fgfrl1*$^{-/-}$ embryos appeared unaffected and the yolk sac had a normal vasculature and blood distribution, but by E14.5 most *Fgfrl1*$^{-/-}$ embryos showed a defect in the septation of the ventricles, which normally completes around this stage (Fig. 5A,D). Expression of *Fgfrl1* in the endocardial cushions of the outflow tract and atrioventricular canal at E10.5 (Fig. 1) suggested a role for *Fgfrl1* in valvulogenesis. Indeed, the leaflets of both the atrioventricular (Fig. 5B,E) and semilunar valves (Fig. 5C,F) were thickened in *Fgfrl1*$^{-/-}$ embryos compared with in wild-type littermates. These defects persisted in E18.5 *Fgfrl1*$^{-/-}$ embryos that developed until term (Fig. 5G-L). Ventricular septation defects and cardiac valve-related congenital heart defects, such as pulmonary stenosis and aortic insufficiency, are characteristic for many WHS patients (Battaglia et al., 2001) and were prominent in *Fgfrl1*$^{-/-}$ embryos (Table 4). Notably, other cardiac defects related to abnormal outflow tract remodelling, such as persistent truncus arteriosus or aortic arch anomalies, were not found in *Fgfrl1*$^{-/-}$ embryos.

Fgfrl1 deficiency causes foetal anaemia

At E12.5, the exchange of oxygen between maternal and foetal blood is established in the labyrinth layer of the placenta when the foetal liver starts producing blood that formerly had been provided by the yolk sac blood islands. Although placental insufficiency could be a primary cause of prenatal lethality in *Fgfrl1*$^{-/-}$ mice, histological analysis of E9.5 and E10.5 placentas from both wild-type and *Fgfrl1*$^{-/-}$ mice showed a proper chorioallantoic fusion in all mice, and at E12.5, the vasculature in the allantois of all *Fgfrl1*$^{-/-}$ mice displayed normal branching in concert with the formation of the chorionic villi (data not shown). By E14.5, there was no gross morphological difference in placental structures between wild-type and *Fgfrl1*$^{-/-}$ mice (Fig. 6A,B), but E16.5 *Fgfrl1*$^{-/-}$ embryos that suffered prenatal lethality showed a clear defect in the placenta (Fig. 6C). The labyrinth layer of the placenta in these mutants was highly disorganized, whereas the placenta in those *Fgfrl1*$^{-/-}$ mice that develop until term did not show any gross morphological defects (Fig. 6D-F). The placental defects in E16.5 *Fgfrl1*$^{-/-}$ embryos that died before birth only appeared after E14.5 when congenital heart defects were already present; therefore, placental phenotypes are

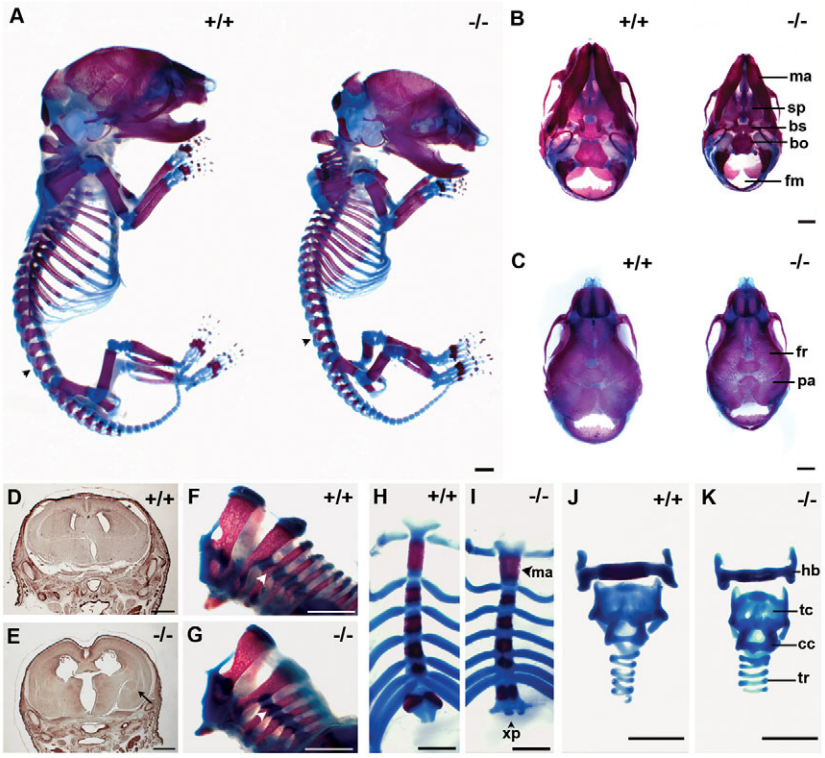

Fig. 4. Skeletal anomalies in *Fgfrl1*$^{-/-}$ embryos. (A) Comparison between the whole skeletons of wild-type (+/+) and homozygous *Fgfrl1* mutant (–/–) embryos at E18.5, with ossified areas in red and cartilage in blue, revealed a general hypoplasia of all skeletal elements in *Fgfrl1* mutant embryos, including shortened axial and appendicular skeletons, malformation of the vertebrae (arrowhead), shortening of the limb girdles and a reduction in the size of the ribcage. (B) Ventral view of the skull, showing midfacial and mandibular hypoplasia and an anterior-shifted foramen magnum in *Fgfrl1*$^{-/-}$ mice. (C) Dorsal view of the skull, revealing a delay in suture closure between frontal and parietal bones in *Fgfrl1*$^{-/-}$ mice. The frontal and parietal bones in *Fgfrl1*$^{-/-}$ mice are also thin compared with those in wild-type littermates. Comparison between cross sections of wild-type (D) and homozygous mutant (E) heads shows enlargement of the brain ventricles and brain overgrowth (arrow) in *Fgfrl1*$^{-/-}$ mice. (F,G) Ossification of the cervical vertebrae (arrowhead) is delayed in homozygous mutants. (H,I) *Fgfrl1*$^{-/-}$ mice display a shortened sternum with abnormal ossification that is most prominent in the manubrium and the xiphoid process. The sternum was also bending inward in the mutant background, contributing to the reduced thoracic diameter. (J,K) *Fgfrl1*$^{-/-}$ mice show incomplete ossification of the hyoid bone and hypoplasia of permanent laryngeal cartilage elements. Abbreviations: bo, basioccipital; bs, basisphenoid; cc, cricoid cartilage; fm, foramen magnum; fr, frontal; hb, hyoid bone; ma, manubrium; pa, parietal; sp, sphenoid; tc, thyroid cartilage; tr, trachea; xp, xiphoid process. Bars, 1 mm.

Table 3. Distance between the proximal and distal growth plates of long bones at E18.5

	Humerus	Ulna	Femur	Tibia
Wt (*n*=11)	2.36±0.11	2.72±0.08	1.97±0.10	2.40±0.09
Fgfrl1$^{-/-}$ (*n*=11)	1.74±0.17*	2.18±0.25*	1.55±0.20*	1.94±0.24*

Long bones of *Fgfrl1*$^{-/-}$ mice were 19-26% shorter than in wild-type mice and this difference was statistically significant.
Mann-Whitney *U* test, *P<0.0001. Length in millimetres (±S.D.).

likely to be secondary to other cardiovascular defects in the cause of prenatal death.

To further investigate the cause of prenatal lethality, we also searched for potential haematopoietic defects. Complete blood count analysis of *Fgfrl1*$^{-/-}$ E16.5 embryos revealed a decrease in red blood cell count (27%), haematocrit (23%) and haemoglobin (37%) (Fig. 7A-C). Although definitive haematopoiesis starts on E12 in foetal mouse liver, the erythroid differentiation process only reaches a steady state after E15.5 (Zhang et al., 2003). To characterise the anaemic state in *Fgfrl1*$^{-/-}$ embryos, we further assessed the maturation stage of foetal liver erythropoiesis by flow cytometry. Although no differences were observed in the absolute counts of foetal liver cells, or cells in the more primitive proerythroblast compartment (c-kit^{+}/Ter119^{-}, CD71^{+}/Ter119^{-}) (Fig. 7D and data not shown), the flow cytometric profile of the mature (Ter119^{+}) cells was affected in *Fgfrl1*$^{-/-}$ E14.5 embryos. An increase in basophilic erythroblasts (R3, 7%) and a decrease in the more mature erythroblasts (R4, 19%; R5, 35%) reflected a delay in the differentiation of erythroid progenitor cells. After two days, *Fgfrl1*$^{-/-}$ E16.5 foetal liver cells showed a normal pattern of erythroid differentiation (Fig. 7D), and at E18.5, peripheral blood displayed normal levels of red blood cells and haemoglobin (data not shown).

DISCUSSION

In this study we present an in-depth characterisation of *Fgfrl1*$^{-/-}$ mice that recapitulate multiple aspects of human WHS. These data support a wider role for *Fgfrl1* in development and implicate *FGFRL1* insufficiency in the human syndrome. Here, the mouse model does not perfectly recapitulate the human syndrome: in human patients, *FGFRL1* haploinsufficiency within the context of a large deletion has been implicated in the craniofacial phenotype of WHS (Engbers et al., 2009), whereas, in the mouse mutants described in the present and previous studies (Baertschi et al., 2007), heterozygous *Fgfrl1* null mutants have no discernible phenotype. Several explanations for this discrepancy can be forwarded. First, developmental processes often involve threshold effects that can be influenced by the genetic background: the literature is rife with examples of null mutations in mice that cause lethal defects on one inbred background, but which are relatively harmless on another (LeCouter et al., 1998; Becker et al., 2003; Teng et al., 2007). In this context, the lack of a phenotype in *Fgfrl1*$^{+/-}$ mice may recapitulate

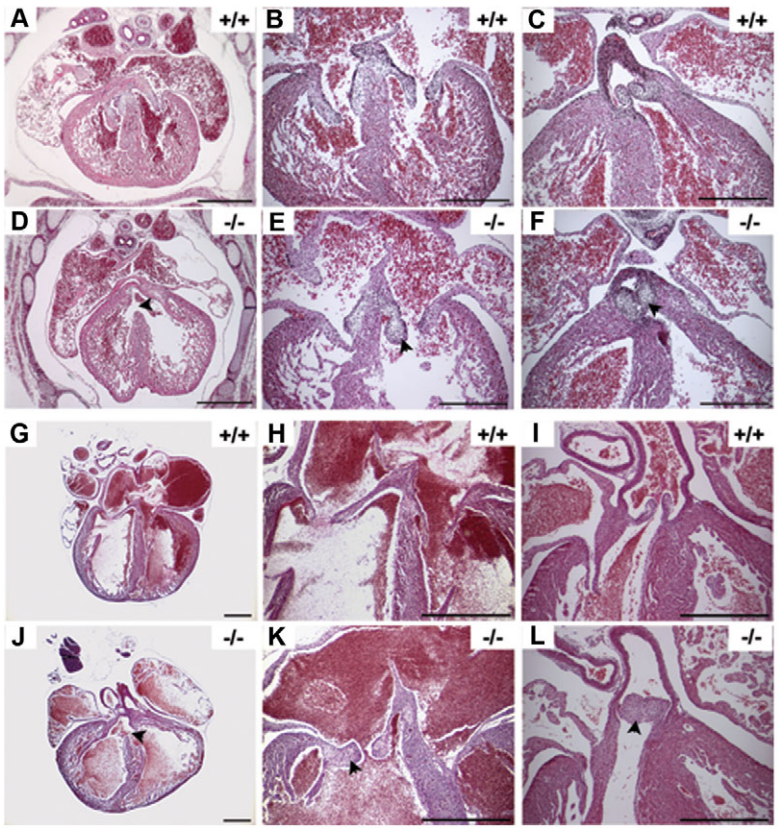

Fig. 5. Congenital heart defects in *Fgfrl1*$^{-/-}$ embryos. At E14.5, a comparison between wild-type (A-C) and *Fgfrl1*$^{-/-}$ (D-F) hearts reveals ventricular septation defects [compare (A) with (D)], and thickening of the atrioventricular [compare (B) with (E)] and semilunar [compare (C) with (F)] valves (arrowheads) in *Fgfrl1*$^{-/-}$ embryos. (G-L) The *Fgfrl1*$^{-/-}$ mutant phenotypes persist at E18.5: ventricular septation defects [compare (G) with (J)], and thickening of the atrioventricular [compare (H) with (K)] and semilunar [compare (I) with (L)] valves (arrowheads). Bars, 0.5 mm.

Table 4. Congenital heart defects in *Fgfrl1*$^{-/-}$ mice at different developmental stages

Cardiac defects	E14.5	E16.5		E18.5
		Severe	Mild	
Membranous VSD	14	7	7	3
Muscular VSD	0	0	0	2
Thickened semilunar valves	16	7	10	8
Thickened atrioventricular valves	16	7	8	3
Thin myocardium	2	0	2	2
Total number of *Fgfrl1*$^{-/-}$ mice	**16**	**7**	**11**	**9**

VSD=ventricular septation defect.

those human genetic backgrounds where the deleterious effects of heterozygous *Fgfrl1* mutations might be masked and go undetected.

Second, in a comparative analysis of WHSCRs, aligning mammalian genes that are orthologous to those at the human 4p16.3 locus (Fig. 8) reveals that, in rodents, this region has been broken up, separating *Fgfrl1* and its neighbouring genes from the WHSCRs over rather distant locations (~75 Mb) on the same chromosome, whereas primates and ungulates maintain a high degree of conservation in chromosomal organisation. A mammalian phylogeny based on molecular data has shown that primates and rodents are more closely linked to each other than to ungulates, which probably represent an ancestral outgroup to the primate-rodent clade (Murphy et al., 2001). The separation of rodent *Fgfrl1* from the WHSCRs may, therefore, be the result of a more recent event, perhaps involving an inversion. This complicates the interpretation of the large-scale mouse deletions, as described by Näf et al. (Näf et al., 2001), since the emerging model of human WHS predicts that many mutations in this region are implicated in the syndrome: deletion of any of at least three non-overlapping regions in 4p16.3 can be pathogenic for the craniofacial features of WHS (South et al., 2008). Thus, it is likely that in humans, heterozygous mutations in both *FGFRL1* and a homologue of an undefined gene that is eliminated in WHS mouse models with large-scale deletions that do not target *Fgfrl1* (Näf et al., 2001), collectively contribute to the craniofacial features of WHS.

Finally, differential regulation of human *FGFRL1* and mouse *Fgfrl1* gene expression may account for the mouse-human differences. In this scenario, the human *FGFRL1* gene may be controlled by proximal regulatory elements that are within the WHSCRs or further towards the centromere; these elements lie distal to the rearranged mouse *Fgfrl1* gene locus, changing the regulatory landscape, thereby exacerbating the effects of haploinsufficiency.

These considerations notwithstanding, *Fgfrl1*$^{-/-}$ mice recapitulate a remarkable number of malformations associated with WHS. Typical WHS skeletal phenotypes (Battaglia et al., 2001) in mutants that develop to term include a short stature, associated shortening of the pelvic girdle and appendicular skeleton, craniofacial dysgenesis, malformed vertebrae, delayed ossification of cervical vertebrae, abnormal sternal ossification and an associated reduction of the thoracic diameter. Laryngeal cartilage elements in *Fgfrl1*$^{-/-}$ mice are significantly reduced in size and provide an explanation for the problems in swallowing and speech development in WHS patients. The fully penetrant diaphragm phenotype of *Fgfrl1*$^{-/-}$ mutants might underlie the diaphragmatic hernia observed in some WHS patients (van Dooren et al., 2004)

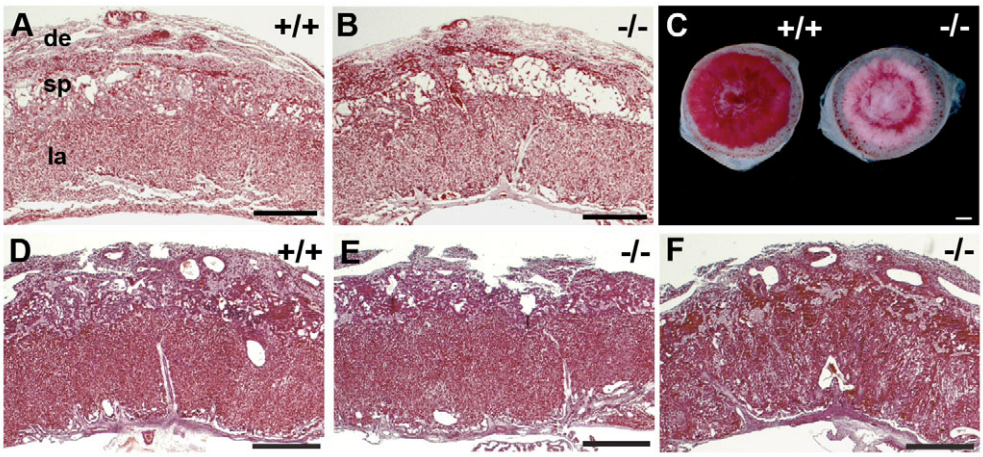

Fig. 6. Comparison of placental development between wild-type (+/+) and homozygous *Fgfrl1* mutant (–/–) embryos. (A,B) Histological analysis of placentas at E14.5 reveals no gross morphological differences between wild-type and *Fgfrl1*$^{-/-}$ embryos. (C) Placentas of severely affected *Fgfrl1*$^{-/-}$ embryos at E16.5 were pale compared with those of wild-type littermates. At E16.5, mildly affected *Fgfrl1*$^{-/-}$ embryos have a normal placenta [compare (D) with (E)], whereas the structure of the labyrinth in placentas of severely affected *Fgfrl1*$^{-/-}$ embryos is highly disorganised (F). Abbreviations: de, decidua; la, labyrinth; sp, spongiotrophoblast. Bars, 1 mm.

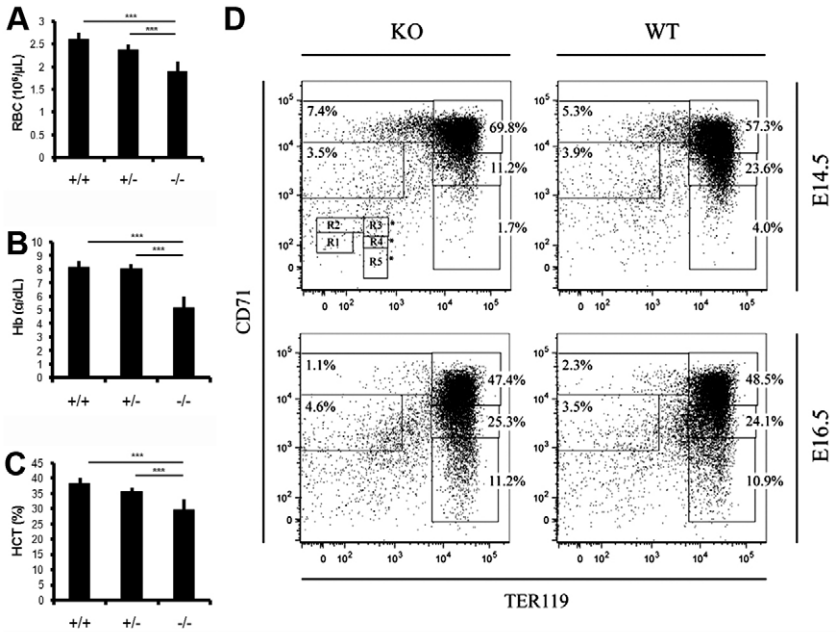

Fig. 7. Foetal anaemia in *Fgfrl1*$^{-/-}$ embryos. (A-C) The peripheral blood in E16.5 *Fgfrl1*$^{-/-}$ embryos shows a 27% decrease in red blood cell count (A), a 37% decrease in the haemoglobin level (B) and 23% less haematocrit (C) compared with wild-type littermates. Data are presented as mean±s.e.m. (***P<0.01). (D) Dot plots of the typical CD71 and Ter119 staining pattern on 10,000 viable cells that were dispersed from wild-type (WT) and *Fgfrl1*$^{-/-}$ (KO) whole foetal livers at E14.5 and E16.5. The axes indicate the relative logarithmic fluorescence units for Ter119-PE-Cy7 (x-axis) and CD71-PE (y-axis). The cells in regions R1 to R5 represent erythroblasts at different developmental stages (R1 contains the least, and R5 the most, differentiated cells) and are defined by their characteristic CD71 and Ter119 staining pattern. These regions can be classified as follows: primitive progenitor cells and proerythroblasts (R1), proerythroblasts and early basophilic erythroblasts (R2), early and late basophilic erythroblasts (R3), chromatophilic and orthochromatophilic erythroblasts (R4), and late orthochromatophilic erythroblasts and reticulocytes (R5) (Zhang et al., 2003). The numbers shown in the boxed areas indicate the frequency of cells in each region, as a percentage of total liver cells. Asterisks indicate the regions (R3, R4, R5) with significantly different values between *Fgfrl1*$^{-/-}$ and wild-type embryos at E14.5 (P<0.01).

and, together with the abnormal laryngeal cartilage elements, contribute to WHS respiratory diseases. *Fgfrl1*$^{-/-}$ mice also display ventricular septation defects and abnormal thickening of both atrioventricular and semilunar valves, in line with common congenital heart malformations, such as pulmonary stenosis and aortic insufficiency, in WHS patients (Battaglia et al., 2001). Together with these cardiac defects, the surviving *Fgfrl1*$^{-/-}$ neonates displayed a combination of congenital malformations including a small rib cage and a fully penetrant diaphragm phenotype that, cumulatively, cause respiratory problems which led to perinatal lethality. By contrast, the *Fgfrl1*-deficient mice generated previously by Baertschi et al. (Baertschi et al., 2007) display the same diaphragm phenotype observed here, but these mice did not reveal any further defects in skeletal or cardiac development. The discrepancy is probably the result of differences in mutant gene construction: in the study by Baertschi et al., the first two exons were removed, potentially preserving partial function of the remaining encoded protein.

The skeletal phenotype of *Fgfrl1*$^{-/-}$ mice at E18.5 is similar to that of the achondroplasia-like dwarfism in transgenic mice that express a constitutively active mutant of MEK1 in chondrocytes, and phosphorylation of MEK1 in the growth plate chondrocytes is caused, at least in part, by signals originating from FGFR3 (Murakami et al., 2004). Interestingly, the *FGFR3* locus, which is proximal to *WHSC1* on the short arm of chromosome 4, has also been cited as a candidate gene contributing to the WHS phenotype (Bergemann et al., 2005). Different missense mutations of human *FGFR3* underlie several skeletal dysplasias, including the most common form of human skeletal dysplasia, achondroplasia, which causes dwarfism (Rousseau et al., 1994; Shiang et al., 1994). In mice, *Fgfr3* is expressed in the proliferating chondrocytes of the growth plate, and gain-of-function mutations, identical to those found in

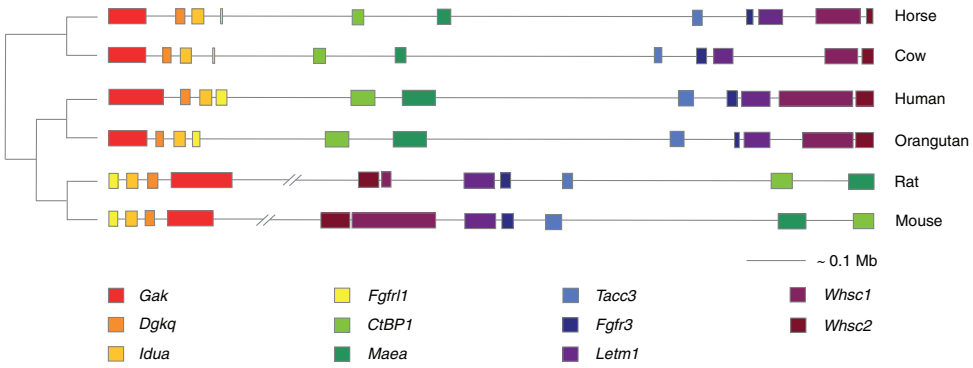

Fig. 8. Comparison between WHSCRs in different mammalian species. Alignment between the human and orangutan (primates), mouse and rat (rodents), and horse and cow (ungulates) orthologous genes, which in humans are located at 4p16.3, reveals a high degree of conservation in chromosomal organisation between primates and ungulates, but shows that rodents have a very different arrangement. The chromosomal region that encompasses a part of 4p16.3 in humans has been broken up in rodents, separating *Fgfrl1* from the WHSCRs over rather distant locations on the same chromosome (~75 Mb in the mouse and ~81 Mb in the rat). (Sequences have been derived from the Ensembl Genome Browser.)

humans, also cause achondroplasia, mimicking the human dwarf phenotype (Naski et al., 1998). By contrast, *Fgfrl1* is specifically expressed in the stem-like cells in the resting zone (Lazarus et al., 2007), which provide the proliferating chondrocytes to the growth plate. The long bones in *Fgfrl1*$^{-/-}$ mice are significantly shorter than in wild-type littermates, whereas *Fgfr3*-deficient mice show bone overgrowth (Colvin et al., 1996). Together, *Fgfrl1* and *Fgfr3* might antagonize each other to control chondrocyte proliferation and it will be interesting to determine whether *Fgfrl1* and *Fgfr3* genetically interact to coordinate bone growth.

Our analysis of the early stages of development revealed that *Fgfrl1* is expressed in the brain, the cranial placodes, the somites and the pharyngeal arches, suggesting that the *Fgfrl1* expression pattern is conserved between mice, Xenopus (Hayashi et al., 2004) and zebrafish (Hall et al., 2006). Zebrafish *fgfrl1a* is also expressed in the arch 1- and 2-associated neural crest, and its depletion results in a craniofacial phenotype, including malformations of the lower jaw and developmental inhibition of the cartilage that is formed by the branchial arches that give rise to the gills (Hall et al., 2006). In mice, the neural crest cells of the first pharyngeal arch form the jawbones and the bones of the face, whereas more posterior pharyngeal arches participate in the development of the hyoid bone and the permanent laryngeal cartilage elements (Noden and Trainor, 2005). *Fgfrl1*$^{-/-}$ mice show a phenotype in all these tissues, implicating *Fgfrl1* in the WHS craniofacial phenotype and a neural crest component in the aetiology of WHS. Similar to *fgfrl1a* in zebrafish (Hall et al., 2006), mouse *Fgfrl1* might control differentiation of post-migratory neural crest cells to complete normal chondrogenesis.

Congenital heart defects at E14.5 probably contribute to prenatal lethality among *Fgfrl1*$^{-/-}$ mice. Expression of *Fgfrl1* in the endocardial cushions of the developing outflow tract might implicate neural crest-derived tissue in these defects. A role for FGF signalling in outflow tract development is illustrated by the persistent truncus arteriosus observed in *Fgf8* mutants (Frank et al., 2002). In addition, congenital heart diseases such as DiGeorge syndrome display persistent truncus arteriosus owing to a 22q11 deletion that results in the loss of *TBX1*, which in mice genetically interacts with *Fgf8* to coordinate cardiac neural crest cells for outflow tract remodelling (Stoller and Epstein, 2005). Our analysis indicates that *Fgfrl1* is not involved in this signalling network, since persistent truncus arteriosus was not present in *Fgfrl1*$^{-/-}$ mice, suggesting that the cardiac neural crest cells that populate the endocardial cushions of the outflow tract were unaffected. Cardiac neural crest cells and endocardial cells both populate the outflow tract cushions, but cardiac valves and part of the ventricular septum are derived from the endocardial cell lineage without a contribution from neural crest cells (de Lange et al., 2004). The specific expression of *Fgfrl1* in the outflow tract and atrioventricular endocardial cushions, in combination with the consistent valve phenotype and ventricular septation defect in *Fgfrl1*$^{-/-}$ mice, support a role for *Fgfrl1* in coordinating cells that are derived from the endocardial lineage to form the valve complexes and to contribute to the ventricular septum.

Further investigation into the potential causes of prenatal lethality led us to focus on the haematopoietic system. At E16.5, *Fgfrl1*$^{-/-}$ mice display anaemia, with the 37% decrease in haemoglobin evidently limiting the oxygen supply to embryonic tissues. The cause for this defect is likely to be the delayed maturation of erythroid progenitors at E14.5. This was a transient problem in *Fgfrl1*$^{-/-}$ mice, because by E16.5 there was no abnormal pattern in liver cell distribution and, at E18.5, normal levels of red blood cells, haematocrit and haemoglobin were observed in the peripheral blood. Nevertheless, persistent haematological disorders have been observed in patients with WHS (Sharathkumar et al., 2003) and our results further support the importance of evaluating children with WHS for haematopoietic dysfunction. Together with cardiac defects, foetal anaemia was present in all *Fgfrl1*$^{-/-}$ mice at E14.5, with no distinction between the potential severely and mildly affected mutants. The varying severity of the combined congenital heart defects and transient foetal anaemia in *Fgfrl1*$^{-/-}$ mice probably represents a stochastic process that underlies the observed prenatal lethality in a portion of mutant embryos.

FGF signalling plays a crucial role in a wide range of developmental processes, including cartilage formation in the vertebrate head (Walshe and Mason, 2003), suture closure (Connerney et al., 2008), bone growth (Kronenberg, 2003) and cardiac valve formation (Sugi et al., 2003). Although the molecular function of FGFLR1 in these processes remains unknown, Trueb et al. (Trueb et al., 2003) have suggested that FGFRL1 might act as a decoy receptor to coordinate the distribution of free FGF ligand. This possibility is supported by the function of the FGFR-related gene *nou-darake* in planarian worms, which is similar to *Fgfrl1* and inhibits FGF signalling in Xenopus eggs (Cebria et al., 2002). Fluorescence resonance energy transfer (FRET) studies demonstrate that FGFRL1 proteins form constitutive homodimers at the cell surface, which promote cell adhesion properties in a similar way to the nectins (Rieckmann et al., 2008). This is consistent with the phenotypic alterations observed in *Fgfrl1*$^{-/-}$ mice, where the absence of *Fgfrl1* may adversely affect epithelial-to-mesenchymal transition of endocardial cells in the outflow tract cushions or the migration of neural crest cells in the pharyngeal arches. Our study thus provides an animal model to investigate mechanistic aspects of mammalian FGFRL1 function that could shed light on the complex aetiology of human WHS disease.

METHODS

Gene targeting

We used homologous recombination to target *Fgfrl1* to produce the *Fgfrl1*^{flox} allele. The targeting construct was generated by inserting part of the *Fgfrl1* locus of a C57BL/6J bacterial artificial chromosome (BAC) clone (BACPAC Resources, CHORI), including a 7.0 kb fragment of intron 2 (5′ arm), exons 3 to 7 (3.1 kb), and a 4.2 kb fragment from downstream of the last exon (3′ arm), into a pBluescript vector by RecE-RecT recombination (Angrand et al., 1999). Generation of *loxP* sites was also performed by using RecE-RecT recombination. A *loxP*-flanked PGK *neo*^{r} cassette was inserted 5′ of exon 3, used for selection and later removed by electroporating positive clones with a Cre-recombinase-expressing plasmid, leaving a single 5′ *loxP* site. The *FRT*-flanked PGK *neo*^{r} cassette and an additional *loxP* site were inserted 3′ of the coding sequence. The final *Fgfrl1* targeting construct was confirmed by sequencing analysis.

The *Fgfrl1* targeting vector was linearised with *Not*I, transfected by electroporation into 129/Sv embryonic stem cells and neomycin-resistant colonies were then screened by Southern blot

hybridisation using 5′ and 3′ external probes with *Spe*I-digested genomic DNA. Additional restriction digests with *Bam*HI and *Eco*RI confirmed the targeting event. Two properly targeted ES cell clones were injected into C57BL/6J blastocysts to generate chimeric mice. Chimeric males were mated with C57BL/6J females and the agouti coat colour, Southern blot and PCR analysis confirmed germline transmission. Heterozygous mice grew normally, and the exons 3 to 7 and the PGK *neo*^{r} cassette were removed in vivo with a CMV-Cre deleter strain (Schwenk et al., 1995). The phenotypes of the two independent lines were similar. Newborn *Fgfrl1*$^{-/-}$ mice were occasionally found half-eaten, which explains why, in many litters, we did not find any *Fgfrl1*$^{-/-}$ mice (see Table 1). Mice with the *Fgfrl1*^{flox} allele and the *Fgfrl1*$^{-/-}$ allele were genotyped by PCR with the primers P1 (5′-CCAGAGTTGTGGGTTCCAG-3′), P2 (5′-GCTGCCTGGGATACACATG-3′) and P3 (5′-GGCATGG-CTGCACTGCTC-3′), using the following parameters: 94°C for 5 minutes, followed by 35 cycles of 94°C for 1 minute, 56°C for 30 seconds and 72°C for 30 seconds. All experiments were performed on mice with a ≥F5 C57BL/6J background and n≥10 unless indicated otherwise. All mouse procedures were approved by the European Molecular Biology Laboratory ethical committee (Monterotondo, Italy) and were in accordance with national and European regulations.

In situ hybridisation

Full-length *Fgfrl1* cDNA in a pCMV-SPORT6 vector (imaGenes) was digested with *Xho*I or *Eco*RI to generate sense and antisense probes, respectively, using a DIG RNA labelling kit (Roche). Embryos were fixed in phosphate buffered saline (PBS)/4% paraformaldehyde (PFA) and stored in methanol. In situ hybridization was performed as described previously (te Welscher et al., 2002). Paraffin sections were counterstained for 5 minutes with Nuclear Red (Vector) and washed in water.

Histological analysis

Embryonic tissues were dissected and fixed in PBS/4% PFA, gradually dehydrated in ethanol and embedded in paraffin. Tissue sections (8 μm) were analysed after Trichrome staining (Sigma-Aldrich).

Quantitative real time (RT)-PCR

Total RNA was prepared from E12.5 embryos using TRIzol (Invitrogen), DNase (Promega)-treated and cleaned by column purification (Qiagen). After quantification by spectroscopy, 2 μg of RNA was used for cDNA synthesis (SuperScript first-strand synthesis system for RT-PCR, Invitrogen). Inventoried FAM TaqMan probes (Applied Biosystems) were used for the relative quantification of the mRNA levels of *Fgfrl1* (Mm01198875_g1), *Fgfr3* (Mm01216080_m1), *Whsc1* (Mm01211108_m1) and *Whsc2* (Mm01217228_m1). Taqman VIC glyceraldehyde 3-phosphate dehydrogenase (*GAPDH*) probes (4352339E) were used for normalisation.

Skeletal staining

E18.5 embryos were skinned and eviscerated before fixation in 95% ethanol overnight. For cartilage staining, embryos were placed overnight in Alcian Blue solution (0.1 g Alcian Blue 8GX in 160 ml of 95% ethanol and 40 ml of glacial acetic acid) and transferred subsequently to 95% ethanol for 3 hours. For bone staining, embryos were cleared in 2% KOH solution for 24 hours and placed overnight in Alizarin Red solution (0.03 g Alizarin Red in 1% KOH solution). Clearing of the embryos was completed in 1% KOH with 20% glycerol for 2 days, and the embryos were then stored in a mixture of ethanol:glycerol (1:1).

Flow cytometric analysis

Single cell suspensions prepared from E14.5 (*Fgfrl1*$^{-/-}$, n=13; wild type, n=7) and E16.5 (*Fgfrl1*$^{-/-}$, n=7; wild type, n=19) foetal livers were filtered (70 μm), washed by centrifugation and resuspended in PBS containing 1% foetal calf serum. Cells were incubated with Fc block (CD16/CD32) for 15 minutes on ice and stained with antibodies for 15 minutes on ice. The antibodies allophycocyanin-conjugated anti-c-Kit, phycoerythrin-conjugated anti-CD71 and PE-Cy7-conjugated Ter119 were obtained from BD Biosciences. Analysis was performed in a two-laser, standard-configuration fluorescence-activated cell sorter (FACS) Canto (BD Biosciences). Gating of the different erythroid populations was performed as described previously (Zhang et al., 2003). Compensation was performed automatically using FACSDiva software 6.0. Data analysis was performed using FlowJo software 8.6 (TreeStar). An

TRANSLATIONAL IMPACT

Clinical issue

Wolf-Hirschhorn syndrome (WHS) is a genetic disorder caused by a partial deletion of the short arm of chromosome 4. WHS patients display a wide variety of phenotypes, but children born with WHS are often diagnosed at birth by characteristic craniofacial features. Other WHS phenotypes include mental retardation, epilepsy, cardiac defects, short stature and skeletal malformations. Haematological disorders and diaphragm defects have also been reported in WHS patients. The genes involved in WHS are not yet known and their identification should help us understand the mechanisms underlying WHS.

Results

In this study, the authors generate a mouse with a loss-of-function mutation in the fibroblast growth factor receptor-like 1 gene (*Fgfrl1*), which is located on the short arm of chromosome 4 in humans. *Fgfrl1* mutant mice recapitulate multiple aspects of WHS, including skeletal malformations and short stature. Additionally, the mouse mutant exhibits abnormal development of permanent laryngeal cartilage elements, providing an explanation for the swallowing problems and impaired speech development observed in humans. *Fgfrl1* null mice also show thickening of the cardiac valves and ventricular septation defects similar to common congenital heart malformations in WHS patients. Other phenotypes reminiscent of WHS that are observed in the *Fgfrl1* mutant mice include diaphragm defects and haematopoietic disorders.

Implications and future directions

This mouse WHS model with a targeted deletion of *Fgfrl1* provides a new tool for studying the genetic mechanisms underlying WHS in humans. Additionally, several forms of cancer and human syndromes that are characterised by craniofacial and skeletal abnormalities are associated with mutations in other FGF receptors. Since FGFRL1 has unique structural characteristics when compared with other FGF receptors, this mouse may provide an insight into the mechanisms of FGF signalling and help explain how FGFRL1 might interact with the other FGF receptors to coordinate the dynamics of different FGF signalling pathways.

doi:10.1242/dmm.003079

equivalent number of events were analysed and displayed graphically in each set of experiments.

Blood analysis

Analysis of peripheral blood was performed with the Drew Scientific Hemavet 950.

Bone measurements

Digital images of long bones were analysed using the MetaMorph software (Version 7.1.2; Molecular Devices).

Statistical analysis

Statistical significance was determined with the unpaired two-tailed Student's *t*-test or with the Mann-Whitney *U*-test, as appropriate for small sample sizes.

URL

The Ensembl Genome Browser is available at http://www.ensembl.org/.

ACKNOWLEDGEMENTS

We are grateful to A. Battaglia and B. Scheres for input and helpful discussions. We thank J. Rientjes, E. Perlas and the members of the EMBL Transgenic Facility for expert help. This work was supported by a long-term fellowship from the HFSPO (P.t.W.), the Leducq Foundation Transatlantic Network for Cardiac Regeneration (P.t.W. and P.K.) and grants from the European Union (Network of Excellence MYORES, grant number: LSHG-CT-2004-511978; Chronic Ulcer Repair and Tissue Regeneration, grant number: LSHB-CT-2005-512102; and Integrated Project HeartRepair, grant number: LSHM-CT-2005-018630).

COMPETING INTERESTS

The authors declare no competing financial interests.

AUTHOR CONTRIBUTIONS

C.C., histological analysis and contributions to experimental design; D.B.-C., flow cytometric analysis; E.S., genotyping; P.K., RT-PCR analysis; N.R., contributions to experimental design and writing of the manuscript; P.t.W., experimental design, histological analysis and writing of the manuscript with input from C.C. and D.B.-C.

Received 21 November 2008; Accepted 6 February 2009.

REFERENCES

Angrand, P. O., Daigle, N., van der Hoeven, F., Scholer, H. R. and Stewart, A. F. (1999). Simplified generation of targeting constructs using ET recombination. *Nucleic Acids Res.* **27**, e16.

Baertschi, S., Zhuang, L. and Trueb, B. (2007). Mice with a targeted disruption of the Fgfrl1 gene die at birth due to alterations in the diaphragm. *FEBS J.* **274**, 6241-6253.

Battaglia, A., Carey, J. C. and Wright, T. J. (2001). Wolf-Hirschhorn (4p-) syndrome. *Adv. Pediatr.* **48**, 75-113.

Becker, D. J., Myers, J. T., Ruff, M. M., Smith, P. L., Gillespie, B. W., Ginsburg, D. W. and Lowe, J. B. (2003). Strain-specific modification of lethality in fucose-deficient mice. *Mamm. Genome* **14**, 130-139.

Bergemann, A. D., Cole, F. and Hirschhorn, K. (2005). The etiology of Wolf-Hirschhorn syndrome. *Trends Genet.* **21**, 188-195.

Beyeler, M. and Trueb, B. (2006). Fgfrl1, a fibroblast growth factor receptor-like gene, is found in the cephalochordate Branchiostoma floridae but not in the urochordate Ciona intestinalis. *Comp. Biochem. Physiol. B* **145**, 43-49.

Bottcher, R. T. and Niehrs, C. (2005). Fibroblast growth factor signaling during early vertebrate development. *Endocr. Rev.* **26**, 63-77.

Cebria, F., Kobayashi, C., Umesono, Y., Nakazawa, M., Mineta, K., Ikeo, K., Gojobori, T., Itoh, M., Taira, M., Sanchez Alvarado, A. et al. (2002). FGFR-related gene nou-darake restricts brain tissues to the head region of planarians. *Nature* **419**, 620-624.

Colvin, J. S., Bohne, B. A., Harding, G. W., McEwen, D. G. and Ornitz, D. M. (1996). Skeletal overgrowth and deafness in mice lacking fibroblast growth factor receptor 3. *Nat. Genet.* **12**, 390-397.

Connerney, J., Andreeva, V., Leshem, Y., Mercado, M. A., Dowell, K., Yang, X., Lindner, V., Friesel, R. E. and Spicer, D. B. (2008). Twist1 homodimers enhance FGF responsiveness of the cranial sutures and promote suture closure. *Dev. Biol.* **318**, 323-334.

de Lange, F. J., Moorman, A. F., Anderson, R. H., Manner, J., Soufan, A. T., de Gier-de Vries, C., Schneider, M. D., Webb, S., van den Hoff, M. J. and Christoffels, V. M. (2004). Lineage and morphogenetic analysis of the cardiac valves. *Circ. Res.* **95**, 645-654.

Engbers, H., van der Smagt, J. J., van't Slot, R., Vermeesch, J. R., Hochstenbach, R. and Poot, M. (2009). Wolf-Hirschhorn syndrome facial dysmorphic features in a patient with a terminal 4p16.3 deletion telomeric to the WHSCR and WHSCR 2 regions. *Eur. J. Hum. Genet.* **17**, 129-132.

Frank, D. U., Fotheringham, L. K., Brewer, J. A., Muglia, L. J., Tristani-Firouzi, M., Capecchi, M. R. and Moon, A. M. (2002). An Fgf8 mouse mutant phenocopies human 22q11 deletion syndrome. *Development* **129**, 4591-4603.

Hall, C., Flores, M. V., Murison, G., Crosier, K. and Crosier, P. (2006). An essential role for zebrafish Fgfrl1 during gill cartilage development. *Mech. Dev.* **123**, 925-940.

Hayashi, S., Itoh, M., Taira, S., Agata, K. and Taira, M. (2004). Expression patterns of Xenopus FGF receptor-like 1/nou-darake in early Xenopus development resemble those of planarian nou-darake and Xenopus FGF8. *Dev. Dyn.* **230**, 700-707.

Kim, I., Moon, S., Yu, K., Kim, U. and Koh, G. Y. (2001). A novel fibroblast growth factor receptor-5 preferentially expressed in the pancreas(1). *Biochim. Biophys. Acta* **1518**, 152-156.

Kronenberg, H. M. (2003). Developmental regulation of the growth plate. *Nature* **423**, 332-336.

Lazarus, J. E., Hegde, A., Andrade, A. C., Nilsson, O. and Baron, J. (2007). Fibroblast growth factor expression in the postnatal growth plate. *Bone* **40**, 577-586.

LeCouter, J. E., Kablar, B., Whyte, P. F., Ying, C. and Rudnicki, M. A. (1998). Strain-dependent embryonic lethality in mice lacking the retinoblastoma-related p130 gene. *Development* **125**, 4669-4679.

Maas, N. M., Van Buggenhout, G., Hannes, F., Thienpont, B., Sanlaville, D., Kok, K., Midro, A., Andrieux, J., Anderlid, B. M., Schoumans, J. et al. (2008). Genotype-phenotype correlation in 21 patients with Wolf-Hirschhorn syndrome using high resolution array comparative genome hybridisation (CGH). *J. Med. Genet.* **45**, 71-80.

Magill, H. L., Shackelford, G. D., McAlister, W. H. and Graviss, E. R. (1980). 4p- (Wolf-Hirschhorn) syndrome. *AJR Am. J. Roentgenol.* **135**, 283-288.

Murakami, S., Balmes, G., McKinney, S., Zhang, Z., Givol, D. and de Crombrugghe, B. (2004). Constitutive activation of MEK1 in chondrocytes causes Stat1-independent achondroplasia-like dwarfism and rescues the Fgfr3-deficient mouse phenotype. *Genes Dev.* **18**, 290-305.

Murphy, W. J., Eizirik, E., Johnson, W. E., Zhang, Y. P., Ryder, O. A. and O'Brien, S. J. (2001). Molecular phylogenetics and the origins of placental mammals. *Nature* **409**, 614-618.

Näf, D., Wilson, L. A., Bergstrom, R. A., Smith, R. S., Goodwin, N. C., Verkerk, A., van Ommen, G. J., Ackerman, S. L., Frankel, W. N. and Schimenti, J. C. (2001). Mouse models for the Wolf-Hirschhorn deletion syndrome. *Hum. Mol. Genet.* **10**, 91-98.

Naski, M. C., Colvin, J. S., Coffin, J. D. and Ornitz, D. M. (1998). Repression of hedgehog signaling and BMP4 expression in growth plate cartilage by fibroblast growth factor receptor 3. *Development* **125**, 4977-4988.

Noden, D. M. and Trainor, P. A. (2005). Relations and interactions between cranial mesoderm and neural crest populations. *J. Anat.* **207**, 575-601.

Rieckmann, T., Kotevic, I. and Trueb, B. (2008). The cell surface receptor FGFRL1 forms constitutive dimers that promote cell adhesion. *Exp. Cell Res.* **314**, 1071-1081.

Rieckmann, T., Zhuang, L., Flück, C. E. and Trueb, B. (2009). Characterization of the first FGFRL1 mutation identified in a craniosynostosis patient. *Biochim. Biophys. Acta* **1792**, 112-121.

Rousseau, F., Bonaventure, J., Legeai-Mallet, L., Pelet, A., Rozet, J. M., Maroteaux, P., Le Merrer, M. and Munnich, A. (1994). Mutations in the gene encoding fibroblast growth factor receptor-3 in achondroplasia. *Nature* **371**, 252-254.

Schwenk, F., Baron, U. and Rajewsky, K. (1995). A cre-transgenic mouse strain for the ubiquitous deletion of loxP-flanked gene segments including deletion in germ cells. *Nucleic Acids Res.* **23**, 5080-5081.

Sharathkumar, A., Kirby, M., Freedman, M., Abdelhaleem, M., Chitayat, D., Teshima, I. E. and Dror, Y. (2003). Malignant hematological disorders in children with Wolf-Hirschhorn syndrome. *Am. J. Med. Genet. A* **119A**, 194-199.

Shiang, R., Thompson, L. M., Zhu, Y. Z., Church, D. M., Fielder, T. J., Bocian, M., Winokur, S. T. and Wasmuth, J. J. (1994). Mutations in the transmembrane domain of FGFR3 cause the most common genetic form of dwarfism, achondroplasia. *Cell* **78**, 335-342.

Sleeman, M., Fraser, J., McDonald, M., Yuan, S., White, D., Grandison, P., Kumble, K., Watson, J. D. and Murison, J. G. (2001). Identification of a new fibroblast growth factor receptor, FGFR5. *Gene* **271**, 171-182.

South, S. T., Hannes, F., Fish, G. S., Vermeesch, J. R. and Zollino, M. (2008). Pathogenic significance of deletions distal to the currently discribed Wolf-Hirschhorn syndrome critical regions on 4p16.3. *Am. J. Med. Genet. C Semin. Med. Genet.* **148C**, 275-280.

Stoller, J. Z. and Epstein, J. A. (2005). Cardiac neural crest. *Semin. Cell Dev. Biol.* **16**, 704-715.

Sugi, Y., Ito, N., Szebenyi, G., Myers, K., Fallon, J. F., Mikawa, T. and Markwald, R. R. (2003). Fibroblast growth factor (FGF)-4 can induce proliferation of cardiac cushion mesenchymal cells during early valve leaflet formation. *Dev. Biol.* **258**, 252-263.

Teng, A., Nair, M., Wells, J., Segre, J. A. and Dai, X. (2007). Strain-dependent perinatal lethality of Ovol1-deficient mice and identification of Ovol2 as a downstream target of Ovol1 in skin epidermis. *Biochim. Biophys. Acta* **1772**, 89-95.

te Welscher, P., Zuniga, A., Kuijper, S., Drenth, T., Goedemans, H. J., Meijlink, F. and Zeller, R. (2002). Progression of vertebrate limb development through SHH-mediated counteraction of GLI3. *Science* **298**, 827-830.

Thisse, B. and Thisse, C. (2005). Functions and regulations of fibroblast growth factor signaling during embryonic development. *Dev. Biol.* **287**, 390-402.

Trueb, B. and Taeschler, S. (2006). Expression of FGFRL1, a novel fibroblast growth factor receptor, during embryonic development. *Int. J. Mol. Med.* **17**, 617-620.

Trueb, B., Zhuang, L., Taeschler, S. and Wiedemann, M. (2003). Characterization of FGFRL1, a novel fibroblast growth factor (FGF) receptor preferentially expressed in skeletal tissues. *J. Biol. Chem.* **278**, 33857-33865.

Trueb, B., Neuhauss, S. C., Baertschi, S., Rieckmann, T., Schild, C. and Taeschler, S. (2005). Fish possess multiple copies of fgfrl1, the gene for a novel FGF receptor. *Biochim. Biophys. Acta* **1727**, 65-74.

van Dooren, M. F., Brooks, A. S., Hoogeboom, A. J., van den Hoonaard, T. L., de Klein, J. E., Wouters, C. H. and Tibboel, D. (2004). Early diagnosis of Wolf-Hirschhorn syndrome triggered by a life-threatening event: congenital diaphragmatic hernia. *Am. J. Med. Genet. A* **127A**, 194-196.

Walshe, J. and Mason, I. (2003). Fgf signalling is required for formation of cartilage in the head. *Dev. Biol.* **264**, 522-536.

Wiedemann, M. and Trueb, B. (2000). Characterization of a novel protein (FGFRL1) from human cartilage related to FGF receptors. *Genomics* **69**, 275-279.

Wiedemann, M. and Trueb, B. (2001). The mouse Fgfrl1 gene coding for a novel FGF receptor-like protein. *Biochim. Biophys. Acta* **1520**, 247-250.

Zhang, J., Socolovsky, M., Gross, A. W. and Lodish, H. F. (2003). Role of Ras signaling in erythroid differentiation of mouse fetal liver cells: functional analysis by a flow cytometry-based novel culture system. *Blood* **102**, 3938-3946.